Diffractive control of 3D multifilamentation in fused silica with micrometric resolution

Omel Mendoza-Yero[1,*], Miguel Carbonell-Leal[1], Carlos Doñate-Buendía[1], Gladys Mínguez-Vega[1] and Jesús Lancis[1]

[1]*GROC•UJI, Institute of New Imaging Technologies, Universitat Jaume I, 12071-Castelló, Spain*
[*]*omendoza@uji.es*

Abstract: We show that a simple diffractive phase element (DPE) can be used to manipulate at will the positions and energy of multiple filaments generated in fused silica under femtosecond pulsed illumination. The method allows obtaining three-dimensional distributions of controlled filaments whose separations can be in the order of few micrometers. With such small distances we are able to study the mutual coherence among filaments from the resulted interference pattern, without needing a two-arm interferometer. The encoding of the DPE into a phase-only spatial light modulator (SLM) provides an extra degree of freedom to the optical set-up, giving more versatility for implementing different DPEs in real time. Our proposal might be particularly suited for applications at which an accurate manipulation of multiple filaments is required.

OCIS codes: (000.0000) General; (000.2700) General science.

References and links

1. W. R. Zipfel, R. M. Williams, and W.W. Webb, "Nonlinear magic: multiphoton microscopy in the biosciences. Nature biotechnology," **21**(11), 1369-1377 (2003).
2. R. Meesat, H. Belmouaddine, J. F. Allard, C. Tanguay-Renaud, R. Lemay, T. Brastaviceanu, L. Tremblay, B. Paquette, J. R. Wagner, J. P. Jay-Gerin, M. Lepage, M. A. Huels, and D. Houde, "Cancer radiotherapy based on femtosecond IR laser-beam filamentation yielding ultra-high dose rates and zero entrance dose," Proc. Nat. Acad. Sci. **109**, E2508-E2513 (2012).
3. R. R. Gattass, and E Mazur, "Femtosecond laser micromachining in transparent materials," Nat. Photonics, **2**(4), 219-225 (2008).
4. V. I. Klimov and D. W . McBranch, "Femtosecond high-sensitivity, chirpfree transient absorption spectroscopy using kilohertz lasers," Opt. Lett. **23**(4), 277-279 (1998).
5. G. Cerullo, and S. De Silvestri, "Ultrafast optical parametric amplifiers," Rev. Sci. Instrum. **74**(1), 1-18 (2003).
6. J. J. Macklin, J . D. Kmetec, and C. L. Gordon III, "High-order harmonic generation using intense femtosecond pulses," Phys. Rev. Let. **70**(6), 766-769 (1993).
7. A. M. Weiner, "Femtosecond pulse shaping using spatial light modulators," Rev. Sci. Instrum. **71**(5), 1929-1960 (2000).
8. S. Hasegawa, Y. Hayasaki, and N. Nishida, "Holographic femtosecond laser processing with multiplexed phase Fresnel lenses," Opt. Lett. **31**(11), 1705-1707 (2006).
9. L. Martínez-León, P. Clemente, E. Tajahuerce, G. Mínguez-Vega, O. Mendoza-Yero, M. Fernández-Alonso, J. Lancis, V. Climent, and P. Andrés, "Spatial-chirp compensation in dynamical holograms reconstructed with ultrafast lasers," Appl. Phys. Lett. **94**(1), 011104 (2009).
10. S. H. Shim, D. B. Strasfeld, E. C. Fulmer, and M. T. Zanni, "Femtosecond pulse shaping directly in the mid-IR using acousto-optic modulation," Opt. Lett. **31**(6), 838-840 (2006).
11. F. Verluise, V. Laude, J. P. Huignard, P. Tournois, and A. Migus, "Arbitrary dispersion control of ultrashort optical pulses with acoustic waves," JOSA B, **17**(1), 138-145 (2000).
12. C. Y. Chang, L. C. Cheng, H. W. Su, Y. Y. Hu, K. C. Cho, W. C. Yen, C. Xu, C. Y. Dong, and S. J. Chen, "Wavefront sensorless adaptive optics temporal focusing-based multiphoton microscopy," Biomed. Opt. Express, **5**(6), 1768-1777 (2014).
13. B. Mills, M. Feinaeugle, C. L. Sones, N. Rizvi and R. W. Eason, "Sub-micron-scale femtosecond laser ablation using a digital micromirror device," J. Micromech. Microeng. **23**(3), 035005 (2013).
14. J. N. Yih, Y. Y. Hu, Y. D. Sie, L. C. Cheng, C. H. Lien, and S. J. Chen, "Temporal focusing-based multiphoton excitation microscopy via digital micromirror device," Opt. Lett. **39**(11), 3134-3137 (2014).

15. O. Mendoza-Yero, V. Loriot, J. Pérez-Vizcaíno, G. Mínguez-Vega, J. Lancis, R. De Nalda, and L. Bañares, "Programmable quasi-direct space-to-time pulse shaper with active wavefront correction," Opt. Lett. **37**(24), 5067-5069 (2012).
16. J. P. Vizcaíno, O. Mendoza-Yero, R. Borrego-Varillas, G. Mínguez-Vega, J. R. Vázquez de Aldana, and J. Láncis, "On-axis non-linear effects with programmable Dammann lenses under femtosecond illumination," Opt. Lett. **38**(10), 1621-1623 (2013).
17. G. Mínguez-Vega, C. Romero, O. Mendoza-Yero, J. R. Vázquez de Aldana, R. Borrego-Varillas, C. Méndez, J. Lancis, P.Andrés, V. Climent, and L. Roso "Wavelength tuning of femtosecond pulses generated in nonlinear crystals by using diffractive lenses," Opt. Lett. **35**(21), 3694-3696 (2010).
18. R. Borrego-Varillas, J. Perez-Vizcaino, O. Mendoza-Yero, G. Minguez-Vega, J. R. Vázquez de Aldana, and J. Lancis, "Controlled Multibeam Supercontinuum Generation With a Spatial Light Modulator," IEEE Photon. Technol. Lett. **26**(16), 1661-1664 (2014).
19. A. Couairon, and A. Mysyrowicz "Femtosecond filamentation in transparent media," Phys. Rep. **441**(2), 47-189 (2007).
20. J. M. Dudley, and S. Coen, "Coherence properties of supercontinuum spectra generated in photonic crystal and tapered optical fibers," Opt. Lett. **27**(13), 1180-1182 (2002).
21. I. Zeylikovich and R. R. Alfano, "Coherence properties of the supercontinuum source," Appl. Phys. B **77**, 265-268 (2003).
22. C. Corsi, A. Tortora and M. Bellini, "Mutual coherence of supercontinuum pulses collinearly generated in bulk media," Appl. Phys. B **77**, 285-290 (2003).
23. C. Corsi, A. Tortora and M. Bellini, "Generation of a variable linear array of phase-coherent supercontinuum sources," Appl. Phys. B **78**, 299-304 (2004).
24. R. Borrego-Varillas, J. Pérez-Vizcaíno, O. Mendoza-Yero, J. R. Vázquez de Aldana, G. Mínguez-Vega, and J. Lancis, "Dynamic Control of Interference Effects between Optical Filaments through Programmable Optical Phase Modulation," J. Display Technol. DOI 10.1109/JDT.2015.2511305 (to be published).
25. C. Romero, R. Borrego-Varillas, A. Camino, G. Mínguez-Vega, O. Mendoza-Yero, J. Hernández-Toro, and J. R. Vázquez de Aldana, "Diffractive optics for spectral control of the supercontinuum generated in sapphire with femtosecond pulses," Opt. Express **19**(6), 4977-4984 (2011).
26. R. Borrego-Varillas, C. Romero, O. Mendoza-Yero, G. Mínguez-Vega, I. Gallardo, and J. R. Vázquez de Aldana, "Femtosecond filamentation in sapphire with diffractive lenses," J. Opt. Soc. Am. B. **30**(8), 2059-2065 (2013).
27. A. Camino, Z. Hao, X. Liu, and J. Lin, "Control of laser filamentation in fused silica by a periodic microlens array," Opt. Express. **21**, 7908 (2013).
28. O. Mendoza-Yero, G. Mínguez-Vega, and J. Lancis, "Encoding complex fields by using a phase-only optical element," Opt. Lett. **39**(7), 1740-1743 (2014).
29. J. A. Davis, and D. M. Cottrell, "Random mask encoding of multiplexed phase-only and binary phase-only filters," Opt. Lett. **19**(7), 496-498 (1994).
30. C. Maurer, S. Khan, S. Fassl, S. Bernet, and M. Ritsch-Marte, "Depth of field multiplexing in microscopy," Opt. Express **18**(3), 3023–3034 (2010).
31. C. Iemmi, J. Campos, J. C. Escalera, O. Lopez-Coronado, R. Gimeno, and M. J. Yzuel, "Depth of focus increase by multiplexing programmable diffractive lenses," Opt. Express **14**(22), 10,207–10,219 (2006).
32. R. D. Leonardo, F. Ianni, and G. Ruocco, "Computer generation of optimal holograms for optical trap arrays," Opt. Express **15**(4), 1913–1922 (2007).
33. David Milam, "Review and assessment of measured values of the nonlinear refractive-index coefficient of fused silica," Appl. Opt. **37**, 546-550 (1998).
34. N. T. Nguyen, A. Saliminia, W. Liu, S. L. Chin, and R. Vallée, "Optical breakdown versus filamentation in fused silica by use of femtosecond infrared laser pulses," Opt. Lett. **28**, 1591-1593 (2003).

1. Introduction

Extremely short temporal light events can be regarded as excellent tools for accessing non-linear optical effects, i.e., self-phase modulation, self-focusing, or plasma generation, due to the combination of spatially focused and femtosecond time scale pulsed light. It is well-known that a suited control over the spatial and temporal properties of ultrashort pulses allows manipulating non-linear phenomena for developing multiple tasks, including two-photon microscopy [1], cancer therapy [2], micro-processing of materials [3], or non-linear spectroscopy [4]. Other settle-down applications i.e., for getting the initial seed in ultrafast optical parametric amplifiers [5], or for synthesizing high harmonics [6] have also been reported. Here, it is apparent that setting specific parameters to ultrashort pulses can be hard to achieve due to several unwanted effects such as temporal dispersion or spatial phase aberrations. In the temporal and/or spatial domains, pulse parameters can be changed in real-time by using optical devices like liquid crystal SLMs [7-9], acoustic-optics crystals [10,11] deformable mirrors [12] or digital micromirror devices (DMDs) [13,14].

On the other hand, the use of diffractive optics has demonstrated its capability to provide not only compact temporal pulse shapers [15], but also to manipulate nonlinear optical phenomena in the axial [16,17], as well as in the transversal direction of the pulse propagation [18]. In this context, we will focus on filamentation [19], which is basically a non-linear propagation phenomenon that is extended a distance longer than the Rayleigh range associated with the pulse. It is originated due to the balance of two main processes, pulse focusing by Kerr effect and defocusing caused by the plasma. Regarding this topic, the coherent nature of the filaments [20] has been investigated by means of several optical setups/devices such as a diffraction-grating-based interferometer [21], collinear geometries with time-delayed pulses [22], variable linear arrays of supercontinuum sources [23] or programmable liquid crystal SLMs [24]. In addition, the filamentation process in fused silica generated under femtosecond illumination has been studied by means of diffractive lenses [24-26]. In particular, conventional arrays of diffractive lenses have been implemented as a tool to generate multiple and predefined filaments in fused silica [24, 27]. At this point, we want to note that the utilization of a conventional array of diffractive lenses for multifilamentation has some drawbacks. The first one is related to the impossibility to bring filaments closer to a distance smaller than twice the physical radius of a lens without using additional optics (assuming arrays of equal lenses). The second drawback comes from the apparent reduction of the numerical aperture of lenses with respect to the numerical aperture of the optical system because of the array implementation itself. Furthermore, the different spatial locations of lenses within an array cause the corresponding focal energies to strongly depend on the initial irradiance distribution of the light source onto the plane of the lens array.

In this contribution we experimentally demonstrate a diffractive-based method to generate arbitrary three-dimensional distributions of filaments in fused silica with accurate control over the spatial locations of filaments. The filaments are originated after focusing femtosecond laser pulses into a fused silica sample by using a single DPE. The encoding of the DPE into phase-only liquid crystal SLM gives additional degrees of freedom to the proposed method, allowing for a dynamic and more versatile operation. In addition, by modulating the phase functions of the lenses we can vary their diffraction efficiency, so modifying the amount of energy employed to produce each filament. Furthermore, due to the characteristics of the encoding method, it is easy to generate filaments with lateral separations in the order of few micrometers. Hence, it will be relatively simple to study the mutual coherence among filaments without using two-arm interferometers or any additional optical components.

The content of the manuscript is organized as follows. In section 2, details of the encoding method are given. In section 3, with the help of a femtosecond laser source and a commercially available SLM, several multifilamentation processes by means of DPEs are experimentally demonstrated. In section 4, we show the usefulness of DPEs to study the mutual coherence among filaments contained within two different spatial distributions. Finally, in section 5 the main conclusions of our work are presented.

2. Basics of the encoding method

In this manuscript a spatially multiplexed procedure is used to encode a set of diffractive lenses into a unique $DPE(x,y)$. With this purpose, the phase information $\Omega_n(x,y)=\mathrm{mod}_{2\pi}\{[(x-x_0)^2+(y-y_0)^2]/(2f_i\lambda_0/\pi)\}$ corresponding to N different off-axis Fresnel lenses, where $n=1..N$, is sampled with N complementary spatially uniform masks $M_n(x,y)$ such as $\sum_{n=1}^{N} M_n(x,y)=1$. The function $\mathrm{mod}_{2\pi}$ holds for the module 2π operation, f_n is the focal lens of the lens n, and variables x and y represent cartesian transverse coordinates. From the above expression, each individual filament located at arbitrary transverse coordinates x_0, y_0 within the fused silica crystal will be originated by the focused light associated with an off-axis kinoform lens also centered at x_0, y_0. In mathematical terms, the resulted $DPE(x,y)$ can be expressed as:

$$DPE(x,y) = M_1(x,y)\Omega_1(x,y) + \ldots + M_N(x,y)\Omega_N(x,y) \quad (1)$$

In order to get further insight into the implementation of this encoding method, we include here a dummy example, see Fig. 1. In the first column of this figure the two-dimensional binary masks $M_n(x,y)$ employed for the sampling process are given. The square gray or black zones within these masks have values one or zero, respectivelly. In practice, each zone will correspond to one pixel of the SLM. For this example the phase functions $\Omega_n(x,y)$ do not represent lenses, but are substituted by the simple patterns shown in the second column of Fig 1. In the right part of Fig. 1, the $DPE(x,y)$ assessed from the sum of sampled functions $\Omega_n(x,y)$, as indicated in Eq.(1), is shown. Hence, it is clear that Fresnel lenses are encoded with different sets of pixels of the SLM. This allows for a separate manipulation of the position and energy coupled into each focus.

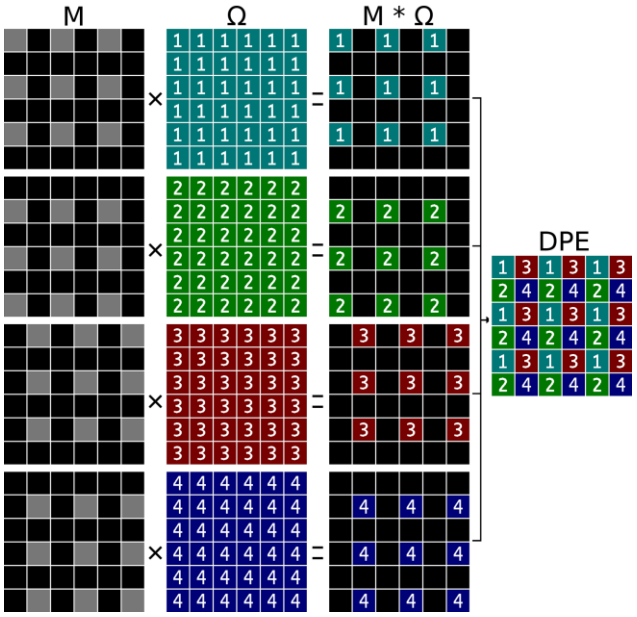

Fig. 1. Dummy example of the encoding method by steps: binary masks (left column), functions to be encoded (middle column), sampled functions (right column), and constructed DPE (right-part).

In contrast, we found that the applicability of this encoding method depends on the accuracy of the sampling process, which is directly linked to the pixel width. Note that, a good sampling process should allows reconstructing the original function by simple extrapolation. So, the number of lenses that can be encoded with this method varies the available pixel width. For a given pupil extension the lower the pixel width the greater the energy at the focal point. In this context, it can be demostrated that the diffraction efficiency quadratic decreases with an increasing number of the superposed Fresnel lenses.

In the literature, similar strategies for spatially multiplexed Fresnel lenses have been reported [28-32]. For instance, it can be metioned a method based on a random sampling of the phase called random mask encoding [31], or another characterized by the application of the weighted Gerchberg-Saxton algorithm [32]. In this manuscript we select a strategy that allows us to carry out a uniform sampling of the phase onto the SLM display. The main reason for doing that is obtaining similar amounts of energy at the focal points of Fresnel lenses even when the laser irradiance at the SLM plane has not a uniform distribution. In addition, as we will shown latter such a spatial multiplexed of lenses is very useful to achieve independent and precise control of the multifilamentation process in bulk.

3. Multifilamentation with DPEs

To experimentally show the ability of DPEs to manipulate at will some parameters of multiple filaments developed in fused silica, we have constructed the optical setup shown in Fig. 2. The light emitted by a Ti: Sapphire femtosecond laser is used as pulsed illumination source. The output pulses are about 30 fs intensity full width at half maximum, with 1 kHz repetition rate, centered at $\lambda_0 = 800nm$ with an approximate energy per pulse of 800 mJ. Before it impinges into the liquid crystal SLM (Reflective PLUTO Phase Only SLM from HOLOEYE), the light is spatially magnified with the help of a 4X reflective optical beam expander (BE04R from Thorlabs). This magnification allows the light to fill the whole area of the liquid crystal display. After that, the light is sent to the SLM via a pellicle beamsplitter (BP145B2 from Thorlabs).

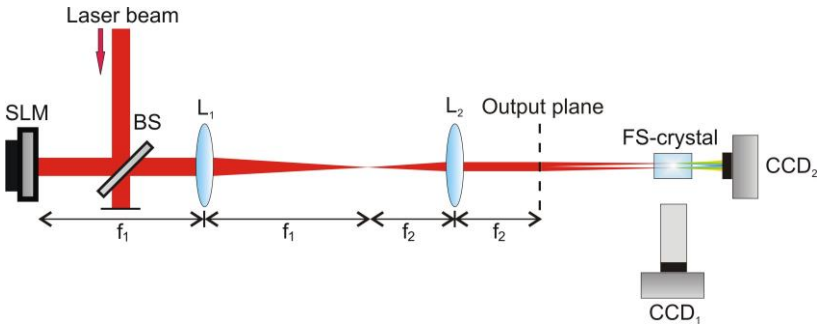

Fig. 2. Experimental setup for the generation of multiple filaments in fused silica with arbitrary spatial distribution and controlled energy by using a single diffractive phase element encoded into a phase-only SLM.

In order to get access to regions very close to the DPE, we form an image of the liquid crystal display with the help of a 4f optical system. This optical system is composed of a couple of lenses with focal lengths $f_1 = 300mm$ and $f_2 = 150mm$. The above combination of lenses decreases by a factor of two the transversal extension of the DPE at the output plane of our imaging system. Accordingly, the magnification of the imaging system in the axial direction is $1/4$. After the output plane of the imaging system, the pulse focuses towards the entrance face of the fused silica crystal (denoted as FS-crystal in Fig. 2), originating a spatial distribution of filaments inside the crystal. Aside, a microscopy objective ($25mm/0.15$NA from Ealing) is used to form an image of the filaments with a magnification of 0.85 onto a CCD camera (model UI-1540SE-M-GL, with resolution 1280x1024 and pixel width 5.2μm from UEYE). Here, we conveniently designed the DPEs to generate spatial distributions of filaments, all of them contained in planes parallels to the plane of the CCD camera. This ensures that, for a given set of experimental parameters i.e., fixed distances among filaments or specific focal lengths for diffractive lenses, all filaments can be recorded at once with the CCD camera. In addition to the above-mentioned camera, another CCD camera (model A102fc, with resolution 1388x1038 and pixel width 6.45μm from Basler) is placed after the rear face of the fused silica crystal in a plane perpendicular to the propagation direction of the filaments, see Fig. 2. This second camera is used to record images originated by the interference of multiple filaments as we will later explain in section 4.

In the present experiment, the focal length of diffractive lenses for the central wavelength of the pulse, λ_0, is $245mm$. However, owing to the 1/4 axial magnification of the 4f optical system, all foci arise in a transversal plane located $61.25mm$ away from the output plane. In addition, the focal energy E_{focal} per diffractive lens is approximately $1.4\mu J$. This energy was determined from the measuring of the average power A_{power} of the pulse at the output plane, just after an iris that fits the pupil of the optical system in this plane. The iris eliminates undesired light reflected from zones of the SLM display outside the pupil. Using the above parameters and taking into account the repetition rate of the laser R_{rate}, and the

theoretical values for the fill factor F_{factor} and diffraction efficiency of our SLM $D_{efficiency}$, the focal energy was calculated by the expression $E_{focal} = A_{power} F_{factor} D_{efficiency} / (N_{lenses} R_{rate})$, where N_{lenses} holds for the number of lenses encoded into the DPE. At this point, E_{focal} can be compared with the energy necessary for generating filamentation. The filamentation regime is achieved if the input power exceeds the critical power obtained from the balance between Kerr self-focusing and plasma defocusing, $P_{cr} = 3.77\lambda_0^2/(8\pi n_0 n_2) = 2.5MW$ where $n_0 = 1.51$ is the refractive index of fused silica for λ_0, and $n_2 = 2.48 \cdot 10^{-20} m^2/W$ is the nonlinear refractive index [33]. Hence, the energy per pulse needed for filamentation can be estimated ($E_{focal\min} = 0.14\mu J$). This means that if all the available energy E_{focal} is employed for non-linear processes, up to 10 additional filaments per encoded lens could be generated. In this context, it has been also shown [34] that for large focal lengths, the threshold energy for filamentation decreases as the corresponding one for the optical breakdown increases. For the parameters used in our experiments, e.g., $f = 245\ mm$, and $E_{focal} = 1.4\mu J$, the filamentation process takes place far away from the optical breakdown, avoiding in this manner modification of the optical parameters or damage of the fused silica sample.

In Fig. 3, recorded images corresponding to four different spatial distributions of filaments within the fused silica crystal are shown. As expected, each distribution of filaments is generated by focusing the light with a specific DPE. To construct the DPEs, we follow the encoding method described in section 2. In all cases, these DPEs are included at the right-part of the filament's images in Fig. 3. Specifically, a set of nine filaments with relative lateral separations of $128\mu m$ are shown in Fig. 3(a). By changing convergent even lenses by highly divergent ones in the previous DPE e.g., with focal length of $-500mm$, another symmetric spatial distribution but this time composed of five filaments with separations of $256\mu m$ was given in Fig. 3(b).

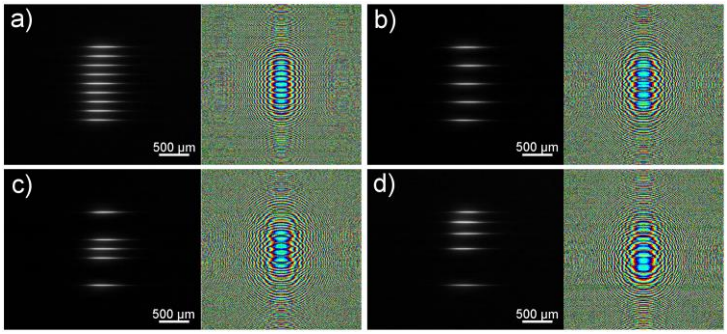

Fig. 3. Recorded images of different spatial distributions of filaments in fused silica due to the focusing of ultrashort pulses with the DPEs shown aside.

Note that, as the light is no longer focused when divergent lenses are used, we can remove the corresponding filaments within the fused silica crystal. Furthermore, for all distances among filaments such that interaction effects can be neglected e.g., like the cases shown in Fig. 3, the encoding method ensures an independent control over the behavior of each filament. With the help of another DPE, a set of five filaments with non-equal separations is achieved in Fig. 3(c). Finally, the potential of the encoding method to generate arbitrary spatial distributions of filaments is experimentally demonstrated in Fig. 3(d). In this last case, a set of five filaments with non-linear increased/decreased distances among them has been obtained.

At this point, it should be noted that both the energy and axial positions of filaments shown in Fig. 3 are almost the same. Small discrepancies in the positions are less than $10\mu m$, which are in the order of the pixel size of our SLM, whereas energy variances are only about 8%. To get this, when necessary, the focal lengths of kinoform diffractive lenses were slightly

modified to correct for unwanted effects due to real experimental conditions. We found that small misalignments of the beam onto the SLM plane led to visible changes of the axial positions of filaments within the crystal. The effect of misalignments can be more clearly seen in Fig. 4 where sets of nine and five filaments achieved without, Fig. 4(a) or Fig. 4(c), and with, Fig. 4(b) or Fig. 4(d), modification of the focal lengths are shown. For instance, when that focal length of all lenses was fixed to $245mm$ we recorded the image given in Fig. 3(c). In contrast, after setting the more convenient focal lenses $f_1 = 245.6\,mm$, $f_2 = 245.0\,mm$, $f_3 = 246.0\,mm$, $f_4 = 245.0\,mm$ and $f_5 = 243.7\,mm$ we got the filament distribution shown in Fig. 4(d). The variable f_i refers to the focal length of the lens i within the DPE.

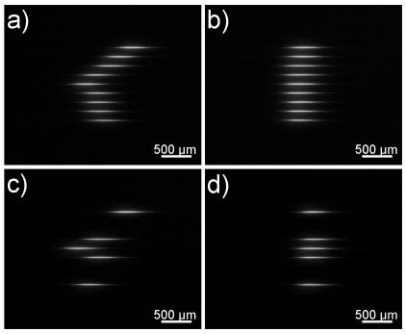

Fig. 4. Images of filaments in fused silica without (a, c) and with (b, d) corrections for the focal lengths and coupled energy.

On the other hand, if required, the focal energy coupled into the filaments can be conveniently decreased to finally obtain a similar amount of energy per filament. To do that, one can change the diffraction efficiency of each lens, modulating its quadratic phases $\Omega_n(x,y)$ with a multiplicative phase parameter δ that ranges from zero to one. In the above expression, the variables x, y represent again transversal coordinates onto the DPE plane. This kind of shaping of the energy distribution per filament may be very useful in situations when the amplitude of the laser beam at the DPE plane evidences clear inhomogeneities. In this case, if a conventional array of lenses is used to focus the pulse like in [24], the amount of energy coupled into the filaments could be quite different. In contrast, distributions of filaments shown in Fig. 3 and 5 have almost the same intensity, so they seem to be not affected by this problem. For this reason, in this experiment corrections were only done in the focal lengths, but not in the diffraction efficiency of lenses. There are other well-known factors i.e., laser beam aberrations [21] or non-uniform spatial phase response [22-24] of the SLM, that also can change energies and positions of foci. However, in our experiment the high temporal stability of the obtained filaments suggests that possible effects introduced by time-dependent factors might be included into the scrambled distribution of filaments already shown in Fig. 4(a) and (c).

Here, it should be mentioned that under broadband spectral illumination each wavelength of the ultrashort pulse is focused by diffractive lenses at different axial positions. Specifically, these positions follow an inverse dependence with the wavelength of light. So, one might expect that filaments generated by focusing ultrashort pulses with diffractive, instead of refractive lenses, show somehow a different behavior due to several reasons. For instance, for the same experimental conditions, i.e., equal numerical aperture, pulse energies and focal lengths, the Rayleigh range due to diffractive lenses is longer than the one obtained by focusing the pulse with a bulk refractive lens. In the temporal domain, basically owing to the propagation time difference among pulses coming from the center and edges of the diffractive lenses, the temporal duration of the pulse at the focus can significantly increase with respect to the temporal pulse width achieved with corresponding refractive lenses. The comparison of the filamentation process obtained with refractive and diffractive optics is

beyond the scope of this manuscript, but a detailed analysis of this topic can be found elsewhere [25].

4. Coherence properties of filaments

In this section we experimentally demonstrate the usefulness of the encoding method to investigate the mutual coherence among filaments developed in fused silica. Note that, the possibility to bring filaments as closer as the pixel width of the SLM can lead to interference effects among them. In this experiment the ultrashort pulse is focused via DPEs into a fused silica crystal to form array of filaments which are able to interfere. The conical emission due to the nonlinear propagation of the pulse within the crystal is superimposed to the interference patterns. The spectral broadening within the visible region of the electromagnetic spectrum originates colored interference patterns whose shapes will depend on the spatial distribution of filaments.

In contrast to a classical two arm interferometer which is usually highly dependent on environmental fluctuations and relatively difficult to align, the use of DPEs allows implementing a compact and robust optical system to measure the visibility of the interference fringes. It is basically composed of a couple of CCD cameras and a SLM. As explained in section 3, the CCD camera placed perpendicular to the propagation direction of the filaments is used to see the straight forward interference patterns, whereas the second camera placed aside the fused silica crystal allows recording the weak plasma emissions or filaments. A complete schematic representation of the optical layout can be seen in Fig. 2. In this optical setup, a suited filter (model KG5, with 25 mm of diameter from Edmund Optics) is utilized to remove non-converted infrared light. For this application, each DPE can be regarded as a programmable single arm interferometer which is poorly dependent on certain unwanted phenomena i.e., mechanical vibrations. Although DPEs cannot be used to significantly vary the delay among pulses that develop in different filaments, the positions of them inside the fused silica crystal if it can be precisely controlled (as demonstrated in section 3). In addition, the energy coupled into the filaments could be also modified by decreasing the above-mentioned phase parameter δ associated with the diffraction efficiency of the lenses. However, owing to the homogeneous spatial sampling of the lenses throughout the DPE, all generated filaments are almost of the same energy, so the need from diffraction efficiency compensation i.e., for instance claimed in [24], is not an issue in the present experiment.

In Fig. 5, the shape of interference patterns for different lateral separations/distances among filaments distributed according to two spatial configurations are shown. The selected distances l among filaments appear as an inset in the right-top part of corresponding images. In the left-bottom part of the images indications of their longitudinal scales are included. Typical longitudinal fringe patterns arise when two filaments interfere, whereas for 3D interference of filaments spot-like patterns come out. In particular, at the left-part of Fig. 5, two similar filaments located approximately at the same axial positions, but having increased/decreased lateral separations between them are shown. The corresponding interference pattern is shown aside. Similarly, at the right-part of Fig. 5, with the same lateral separations as before and following the 3D spatial distribution, images of three filaments and their interference patterns are shown. These three constituent filaments are located in the vertices of an equilateral triangle. In this case, note that visible variations in the intensity of filaments are mainly due to locations of filaments at different planes within the triangular distribution. As it might be expected, the longer the distance among filaments the more magnified the interference pattern will be. In addition, one can see that interferences patterns are color-dependent. We found out that the distribution of colors within the interference patterns changes with the penetration depth of filaments within the fused silica crystal. This effect seems to be related to two main factors, the change of chromatic aberrations at the focal regions achieved for different focal lengths, and the variation in the amount of material dispersion introduced by the crystal for different penetration depths.

On the other hand, it is apparent that changes in the lateral distance among filaments should not alter the visibility of the interference pattern. In fact, from Fig. 5 one can roughly

see that the contrast of interference patterns is more or less the same in all cases. This guarantees a high coherence among the different filaments. However, this is not longer true when variations of distances take place in the axial instead of the lateral direction to the propagation direction of the filaments.

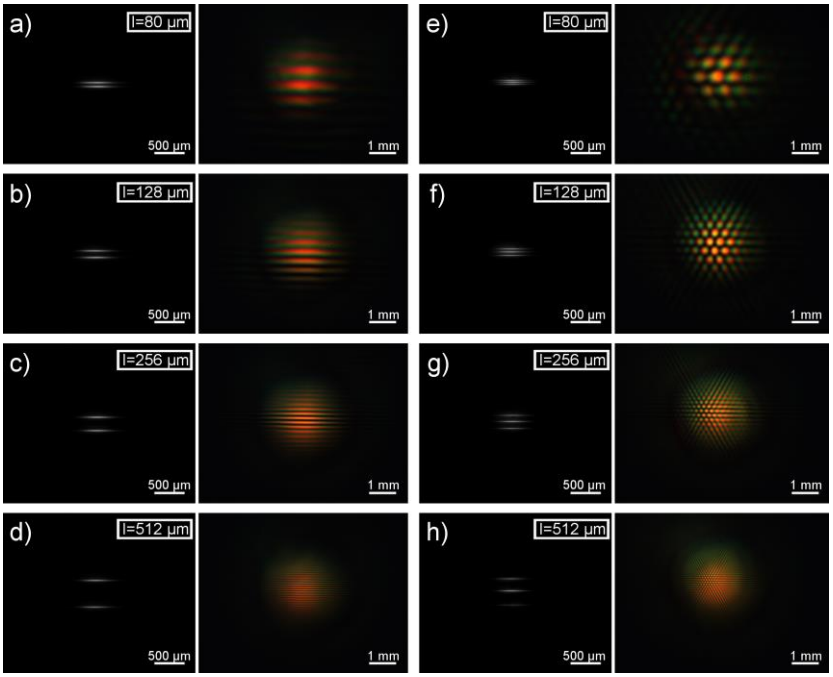

Fig. 5. Images of filaments with corresponding interference patterns for different lateral separations and spatial distributions. (a-d) two filaments located at the same plane (e-h) three filaments located in the vertexes of an equilateral triangle.

In the next experiment we want to show that using DPEs it is possible to investigate the effect of the axial separation of two filaments on the visibility of the interference pattern. Our experimental results are shown in Fig. 6. The axial distances d shown as insets in the right-top part of Fig. 6(a-e) are taken with respect to the upper filament which is kept fixed. To change the distance between filaments, the focal length of the diffractive lens associated with the lower filament was ranged from $241.8\,mm$ to $248.0\,mm$ by means of variable increments. As the interference patterns are color-dependent, different visibility values were calculated for each image corresponding to the red, green and blue (RGB) channels of the camera. These visibility values were determined for a couple of central fringes, using an irradiance profile taken at the middle of each interference pattern. These irradiance profiles (also plotted with red, green and blue colors) are shown in the right-part column of Fig. 6, together with the corresponding three values of visibility added as insets. For comparison, all visibility values were normalized with respect to the value achieved with the red channel in Fig. 6(c). This maximum value corresponds to the situation when there is no separation between upper and lower filaments. In this case, the visibility assessed due to the remaining channels is also the greatest. Therefore, the visibility worsens while increasing the axial separation between filaments. In these cases, the optical path and the delay between both filaments is no longer zero because original infrared pulses pass through different amounts of material dispersion.

The experimental results shown in Fig. 6 also reveal that apart from the apparent changes of visibility with the axial separation of filaments, there is an additional factor that could be taken into account. This factor is the different behavior of the visibility parameter for each RGB image of the interference pattern. For instance, for the experimental parameters used to get Fig. 6 i.e., penetration depths of filaments within the crystal of about 4 mm or focal

lengths around $245.0\,mm$, the values of visibility achieved with the red channel are less affected by variations of the axial position of filaments than corresponding values due to the remaining channels. However, after changing the penetration depth of filaments within the crystal, the behavior of visibility parameter for each RGB images also varies. We found that, among other reasons, this phenomenon is linked to the visible change in the azimuthal distribution of colors within the interference pattern due to the modification of the penetration depth.

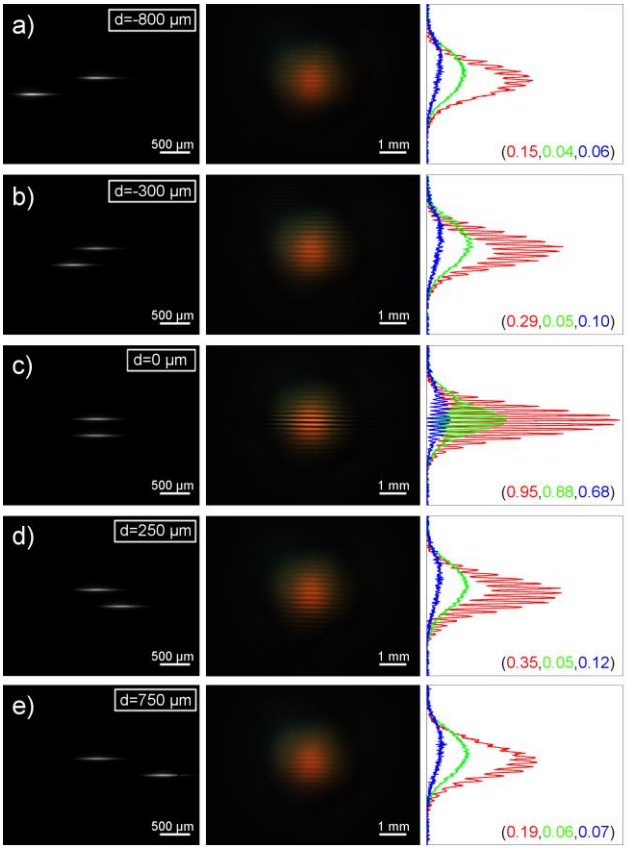

Fig. 6. Images of filaments (left-column) with corresponding interference patterns (middle column) together with their RGB central profiles (right-column) for different axial separations.

In order to show this effect, a set of interference patterns obtained for three different penetration depths (included with the variable p in their top-right parts) are shown in Fig. 7. In this experiment, the interference patterns were originated by the interaction of a couple of filaments having lateral ($l = 216\mu m$), but not axial ($d = 0$) separations between them.

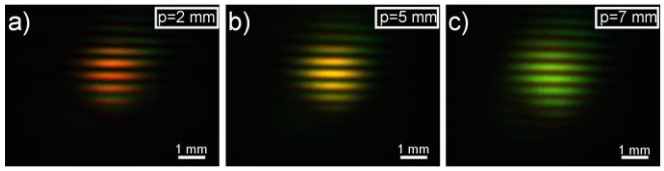

Fig. 7. Interference patterns due to the interaction of a couple of filaments for different penetration depths within the fused silica crystal.

To introduce approximatelly the same amount of chromatic aberrations, the focal length ($f = 280mm$) of the two diffractive lenses employed to generate the filaments remains the same during the whole experiment. Instead, with the help of a motorized stage, the fused silica

crystal was moved with respect to the filaments. After a visual inspection of Fig. 7, one can conclude that the predominant color within the interference patterns is shifted when modifying the penetration depth. In the time domain, increasing/decreasing the material dispersion implies variations in the temporal width of the pulse, which influence the development of filaments within the crystal, as well as the characteristics of corresponding interference patterns, see Fig.8.

5. Conclusions

In this manuscript, we experimentally showed that DPEs encoded into a phase-only SLM can be successfully utilized to generate arbitrary 3D spatial distributions of filaments in bulk optics with micrometric spatial resolution. The spatial sampling procedure employed to construct each DPE allows having high accuracy and independent control over some physical parameters of filaments such as the energy coupled into the filaments or their positions within the fused silica crystal. We found that both the coupled energy and the relative positions of filaments can be conveniently tuned by changing the diffraction efficiency, and the center of the corresponding off-axis kinoform diffractive lenses, respectively. The usefulness and robustness of DPEs for practical applications were tested with a couple of experiments addressed to study the mutal coherence of filaments while they develop inside the fused silica crystal. In particular, we showed that visibility of interference patterns due to the interaction of filaments within a predefined spatial distribution changes when modifying the relative axial distances among filaments. Its maximum value is achieved when there is no axial separation between filaments. In addition, for a selected pair of fringes we found that the visibility also depends on the RGB image associated with the interference pattern.

In comparison with previous studies aimed to the control of multifilamentation processes in fused silica by using arrays of diffractive lenses, our proposal showed some advances. The most significant one is the possibility to bring filaments as close as the pixel width of the SLM without using additional optical components. Another advance is the tested ability of DPEs to generate filaments with relative similar energies, regardless the homogeneity of the beam's irradiance onto the DPE. These advances are made possible mainly due to the homogeneous spatial sampling of the diffractive lenses, which also guarantees high numerical aperture for the mix of lenses. However, with the encoding method used in this manuscript one can encode only a limited amount of lenses, basically because the sampling of the phase associated with each lens gets worse when increasing the number of lenses in the DPE. This drawback might be softened if technology behind the next generation of SLMs allows for devices with better resolution and lower pixel width.

Acknowledgements

We acknowledge support from Generalitat Valenciana through the programme PROMETEO-2012-021, University Jaume I through the project P1·1B2013-53, and Ministerio de Economía y Competitividad (MINECO) through the project FIS2013-40666-P. The authors are also very grateful to the SCIC of the Universitat Jaume I for the use of the femtosecond laser.